SCIENTIFIC REPORTS

OPEN

SUBJECT AREAS:
MAGNETIC PROPERTIES AND MATERIALS
TWO-DIMENSIONAL MATERIALS

Received
29 April 2014

Accepted
22 July 2014

Published
14 August 2014

Correspondence and requests for materials should be addressed to J.H. (hongj@pknu.ac.kr)

Transparent half metallic g-C_4N_3 nanotubes: potential multifunctional applications for spintronics and optical devices

Tao Hu, Arqum Hashmi & Jisang Hong

Department of Physics, Pukyong National University, Busan 608-737, Korea.

Multifunctional material brings many interesting issues because of various potential device applications. Using first principles calculations, we predict that the graphitic carbon nitride (g-C_4N_3) nanotubes can display multifunctional properties for both spintronics and optical device applications. Very interestingly, armchair tubes (n, n) with n = 2, 3, 4, 5, 6 and (5, 0) zigzag tubes are found to be half metallic, while zigzag tubes (n, 0) with n = 4, 6 show an antiferromagnetic ground state with band gaps. However, larger zigzag tubes of (7, 0), (8, 0), and (10, 0) are turned out to be half metallic. Along with the half metallic behavior of the tubes, those tubes seem to be optically transparent in the visible range. Due to these magnetic and optical properties, we suggest that the g-C_4N_3 nanotubes (CNNTs) can be used for both ideal spintronics and transparent electrode materials. We also explored the stability of magnetic state and nanotube structure using *ab initio* molecular dynamics. The CNNTs were found to be thermally stable and the magnetic moment was robust against the structural deformation at 300 K. Overall, our theoretical prediction in one dimensional CNNTs may provide a new physics in spintronics and also in other device applications because of potential multifunctional properties.

Half metallic system is of particular interest in spintroincs because one spin channel is completely suppressed at the Fermi level and due to this feature many technical difficulties for device applications can be avoided. In particular, magnetism arising from pure 2p electron system without any 3d transition metal elements can bring great advantage for spintronics. For instance, a spin relaxation time is one of the key factors in spintronics and it is inversely proportional to spin orbit coupling. Thus, relatively long spin relaxation time is expected from 2p electron systems because of weak spin orbit coupling compared with the strength of spin orbit coupling found in conventional 3d transition metal systems.

Regarding the 2p magnetism, considerable efforts have been devoted towards the synthesis, characterization, and magnetism discovery in g-C_3N_4 system[1–4]. However, the g-C_3N_4 was found to be non-magnetic[5,6]. In 2010, a similar graphitic carbon nitride material so called g-C_4N_3 was synthesized[7]. Recent study showed that a ferromagnetic ground state could be found in two dimensional g-C_4N_3 sheet[8], and several works have been reported[9–14]. Since the g-C_4N_3 consists of purely 2p elements, it will be of interest if one can obtain metal free half metallic state in nanotube structures and we believe that it will be possible to synthesize g-C_4N_3 nanotubes (CNNTs) using the experiences obtained from carbon nanotubes fabrication study. Indeed, one can easily find numerous studies on one dimensional g-C_3N_4 nanotubes[15–17] and these g-C_3N_4 nanotubes are found to be non-magnetic semiconductor. Unlike many studies on g-C_3N_4 nanotubes, no report has been presented so far for the possibility of metal free half metallic state and optical properties in one dimensional CNNTs systems. Herein, we show that the half metallic behavior can be observed in CNNTs and the relationship between magnetism and chirality of CNNTs are investigated as well. In addition, the thermal stability of tubular structures and robustness of ferromagnetic state at room temperature are explored using *ab initio* molecular dynamics. Furthermore, the frequency dependent dielectric function and energy dependent absorption coefficient for optical property are calculated. With these studies, our objective is to propose that the g-C_4N_3 nanotubes can be utilized as potential multifunctional materials for both spintronics and optical device applications.

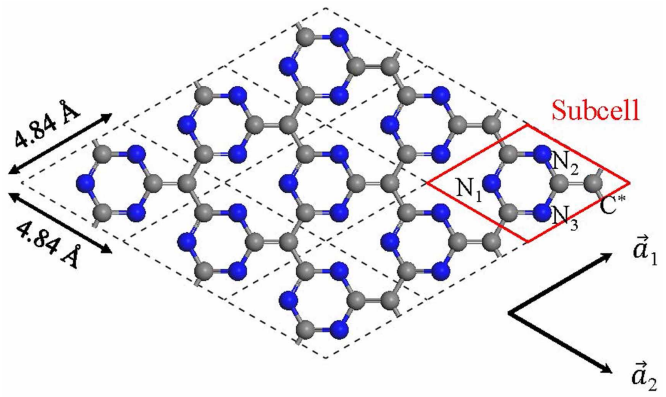

Figure 1 | Schematic illustration of two dimensional g-C_4N_3 layer. Here, $\vec{a}_1$ and $\vec{a}_2$ are lattice vectors.

Results

The CNNTs considered in our calculations are based on two dimensional g-C_4N_3 layer in the perspective of the geometry as shown in Fig. 1. The part depicted in red region is a unit cell of g-C_4N_3 which contains four C atoms and three N atoms. A carbon atom located out of the hexagonal ring is denoted by C* and three other N atoms are represented by N_1, N_2, and N_3. Fig. 2 (a)–(h) shows the optimized configurations of CNNT systems. All the tubes are found to be nearly round shape except (2, 2) armchair tube. In this particular (2, 2) armchair tube, it appears like a square with a parameter of 5.09 Å. A diameter of the tube can be determined by chirality index and an approximated diameter of tube is indicated. Besides this diameter, the length of unit cell also controls the structure of the tube. For armchair tubes, the length of one unit cell was about 4.85 Å in (2, 2) case and it is almost unchanged in other armchair tubes. In zigzag tubes, the length was 8.31 Å in both (4, 0) and (6, 0) tubes, whereas it became 8.38 Å in (5, 0). For larger tubes of (7, 0), (8, 0) and (10, 0) indices, it was 8.38 Å and these zigzag tubes whose diameter is larger than 10.7 Å show a buckling behavior as found in a two dimensional layer[8].

In each structure, we considered three magnetic states such as ferromagnetic (FM), antiferromagnetic (AFM), and non-magnetic (NM) states and total energy calculations were performed. Note that the structure optimization has been performed in each spin configuration. The total energy of FM state was set to zero as a reference energy. In Table 1, we present the calculated total energy differences. First of all, the armchair CNNTs have always FM ground state. However, in small size of zigzag tubes, the magnetic ground state fluctuates as the diameter of the tube changes. For instance, both (4, 0) and (6, 0) zigzag CNNTs were found to be more stable in the AFM state than the other spin states. In contrast, the FM state was obtained in (5, 0) tube. Interestingly, we found FM ground state in (7, 0), (8, 0), and (10, 0) zigzag tubes. From the calculated results of 11 different tubes, we propose a hypothetical rule for magnetism of CNNTs. The armchair tube always prefers FM state, while the zigzag tube of (n, 0) index manifests FM ground state if n is larger than 6. Of course, further investigation is required to verify the rule for magnetism. We also calculated magnetic moment of each tube. In FM state, both armchair and zigzag tubes of (n, n) and (n, 0) indices have magnetic moment of 2n μ_B. Since there are 2n block subcells in each tube, the magnetic moment per subcell becomes 1 μ_B. In AFM state, each subcell maintains magnetic state, but the net magnetization completely vanishes due to the opposite spin polarization in the neighboring subcells. Note that the calculated magnetic moment per cell in a two dimensional layer is 1 μ_B. This result implies that the magnetic moment per subcell seems very robust despite dramatic changes in geometric structure. In addition, the integer magnetic moment implies that the CNNTs have half metallic characteristics. In structural point of view, the CNNT will gradually transform into two dimensional layer structure as the diameter of the tube increases and finally the CNNT will show the same magnetic property found in two dimensional layer system. In our calculations, we clearly proposed the critical diameter of tube which showed the half metallic ground state regardless of the chirality. Overall, the CNNTs show chirality independent half metallic state when the diameter of the

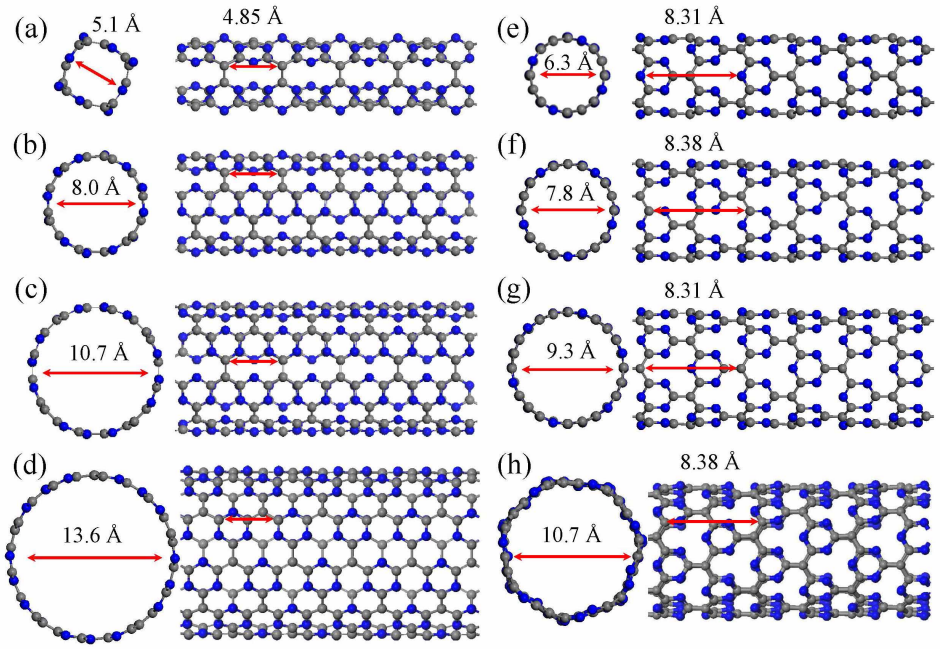

Figure 2 | Top and side views of optimized structure CNNTs: (a)–(d) for armchairs of (n, n) with n = 2, 3, 4 and 5, respectively and (e)–(h) for zigzag tubes of (n, 0) with n = 4, 5, 6 and 7, respectively. Other tubes considered in our work have similar structure. The only difference is the number of subcells and the diameter.

Table 1 | Calculated total energy differences (in meV) of CNNTs

Index	(2, 2)	(3, 3)	(4, 4)	(5, 5)	(6, 6)	(4, 0)	(5, 0)	(6, 0)	(7, 0)	(8, 0)	(10, 0)
FM	0	0	0	0	0	0	0	0	0	0	0
AFM	250	370	460	601	807	−180	665	−540	838	202	251
NM	360	380	490	617	726	810	786	980	834	929	984

tube is larger than a certain critical value and this finding will be definitely favorable for spintronics applications in various ways.

We now present the calculated spin magnetic moments of N and C atoms inside Wigner-Seitz radius of 0.863 Å for N and 0.741 Å for C, respectively in Table 2. It is observed that the spin polarization mainly originates from N atoms, whereas the C atoms do not show meaningful spin polarization, except (2, 2) armchair tube. In (2, 2,) tube the carbon atom, which is located out of the hexagonal ring (C*), was found to be spin polarized and this is due to an unusual geometric feature of (2, 2) armchair tube. As depicted in Fig. 1, there are three N atoms. Both N_2 and N_3 atoms were found to have the same magnetic moment in FM tubes, while the three N atoms were inequivalent in AFM tubes. Very interestingly, the integer number of magnetic moment per subcell is obtained if we include the contribution to the magnetic moment from interstitial part and this implies that the system becomes half metallic material.

Fig. 3 shows the calculated electronic band structure of CNNTs. Indeed, we noticed that the band structures of (5, 5), (6, 0) and (10, 0) tubes were similar to those of (6, 6), (4, 0) and (8, 0), respectively, thus they are omitted in Fig. 3. In armchair tubes, as indicated from the calculated magnetic moment per subcell, one can clearly see half metallic state because the occupied majority spin bands are completely located below the Fermi level, while the minority spin bands cross the Fermi level. The same half metallicity is observed in zigzag tubes as well, except for (4, 0) and (6, 0) tubes. The calculated band gaps in majority spin bands are 2.26, 1.99, 2.05, 2.11, 2.16, 1.78, 2.08, 2.11. and 2.07 eV for the tubes (2, 2), (3, 3), (4, 4), (5, 5), (6, 6), (5, 0), (7, 0), (8, 0), and (10, 0) respectively. In (4, 0) and (6, 0) tubes, the band gaps are observed and they are 0.27 and 0.28 eV, respectively. Therefore, (4, 0) and (6, 0) zigzag tubes are semiconductors. In Fig. 4, we present calculated total density of states (DOS). As indicated in band structures, the DOS also clearly shows half metallic behavior in armchair tubes and (5, 0), (7, 0), and (8, 0) zigzag tubes, whereas band gap is found in (4, 0) tube. By further analyzing the calculated DOS of each tube, we have observed that the contribution to magnetism originates from *p* orbitals and the spin polarized orbitals depend on chirality and tube structures. Moreover, we have extracted the information on the localized orbitals which are responsible for the magnetic moment. In (3, 3), (4, 4), (5, 5) and (6, 6) armchair tubes which have cylinder shapes, both axial orbitals of N_2 and N_3 (equivalent to N_2) atoms and tangential orbital of N_1 atom mainly contribute to the magnetic moment. In (2, 2) tube, which is close to square tube, axial orbital of N_2 and N_3 atoms and radial orbital of C* atom mainly contribute to the magnetic moment. However, in zigzag tubes like (5, 0), (7, 0), (8, 0) and (10, 0), both axial and radial orbitals of N_1 contribute to the magnetic moment. Comparing both orbitals, we found that the axial orbital contribution was relatively stronger. In N_2 and N_3 atoms, both tangential and axial orbitals play an essential role for the magnetism. In this case the tangential component contributed to the magnetic moment a little bit more than axial component.

To investigate the thermal stability and the existence of magnetic state, spin-polarized *ab initio* molecular dynamics simulations were performed at 300 K and 500 K up to 10 ps for (4, 4). The CNNT tube structures at both 300 K and 500 K are shown in Fig. 5. At 300 K, the essential tube structure is intact, even though a small distortion is found and the magneitc state remains with an average magnetic moment of 8 μ_B. Note that this temperature has nothing to do with the critical temperature because the *ab initio* molecular dynamics does not include spin dynamics. Nonetheless, we find that the magnetic state is very robust against the structural deformation. The thermal stability at 500 K was also checked. The tube structure was deformed significantly, and it tends to convert into two connected plain surfaces due to strain of nanotube geometry. Furthermore, the subcell structure is destroyed because of large displacement of some atoms, and pentagon circles appear. The geometry is not a construction from the subcell anymore. This indicates that the tube structure is not thermally stable at 500 K.

Along with the half metallic properties found in CNNTs, the CNNTs systems will attract extensive research interest as a multifunctional material if the CNNTs can be utilized for device applications using optical properties. Thus, it will also be of interest to investigate optical properties of CNNTs. To this end, we have calculated frequency dependent dielectric function $\varepsilon(\omega) = \varepsilon_1(\omega) + i\varepsilon_2(\omega)$ for optical properties. From this dielectric function, the absorption coefficient (α(E)) as a function of photon energy (E(eV)) can be obtained using the following formula:

$$\alpha(E) = \frac{2\pi E(eV)}{\hbar c}\sqrt{\frac{\sqrt{\varepsilon_1^2(\omega)+\varepsilon_2^2(\omega)}-\varepsilon_1(\omega)}{2}} \qquad (1)$$

The real and imaginary parts of dielectric function is related by well-known Kramers-Kronig relations, we thus only present imaginary part of dielectric functions in Fig. 6 (a) and (b) for both perpendicular and parallel polarization to the tube axis. Since the intensity of imaginary part of the dielectric function in parallel polarization is larger than that in perpendicular polarization, we expect optical anisotropy for absorption coefficient according to the polarization. From the band calculated structure results, one can easily find that the contribution to dielectric function due to intraband transition can be ignored if the photon energy is larger than approximately 0.5 eV. Thus, we have realized that the interband transition plays an essential role in the wide range of photon energy for the frequency dependent dielectric function. For optical device applications, it is of interest to

Table 2 | Calculated spin magnetic moment (in μ_B) inside Wigner-Seitz radius

Index	(2, 2)	(3, 3)	(4, 4)	(5, 5)	(6, 6)	(4, 0)	(5, 0)	(6, 0)	(7, 0)	(8, 0)	(10, 0)
C*	0.24	0.05	0.03	0.03	0.03	±0.05	0.05	±0.05	0.10	0.11	0.02
N_1	0.08	0.20	0.24	0.24	0.25	±0.10	0.29	±0.10	0.28	0.27	0.26
N_2	0.22	0.27	0.26	0.26	0.26	±0.18	0.23	±0.20	0.24	0.24	0.25
N_3	0.22	0.27	0.26	0.26	0.26	±0.27	0.23	±0.23	0.18	0.18	0.26

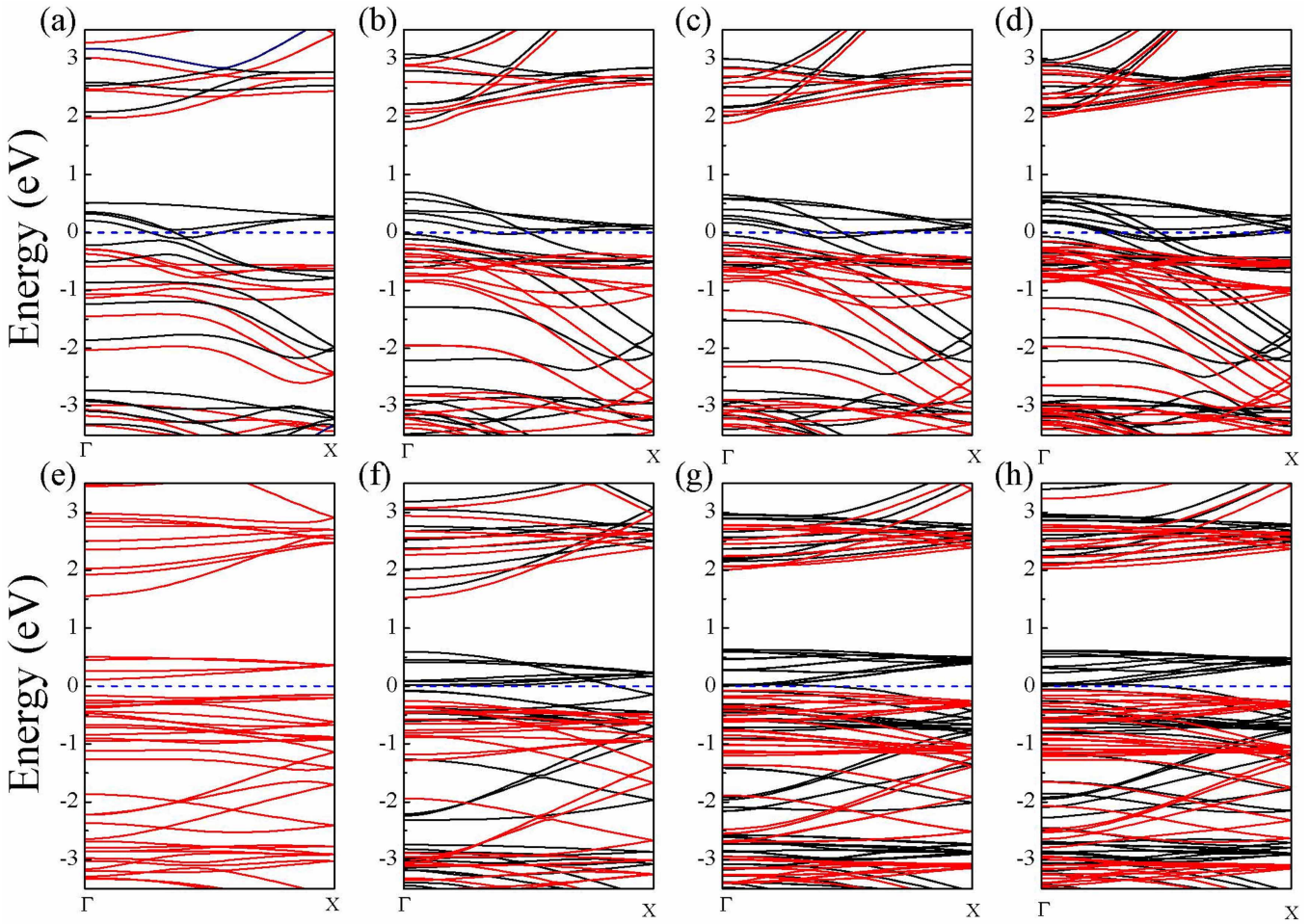

Figure 3 | Calculated energy band structures: (a)–(d) are for (2, 2), (3, 3), (4, 4) and (6, 6) armchair tubes, respectively and (e)–(h) are for (4, 0), (5, 0), (7, 0) and (8, 0) zigzag tubes, respectively. The red lines represent majority spin bands and the blacks lines are for minority spin bands. The Fermi level is indicated in blue dashed line.

focus on the absorption coefficients in the visible ranges. Using the relation presented in the above, the energy dependent absorption coefficients are shown in Fig. 7 (a) and (b) for both polarization directions. The intensity of traveling light will decay exponentially as a function of distance. Thus, one can find that the attenuation of traveling visible light is very weak and this, in turn, implies that the CNNTs are likely to be optically transparent. Thus, the CNNTs may have potential applications for transparent electrode as well as spintronics materials.

Discussion

We have investigated magnetic and optical properties of CNNTs by using density functional calculations. Interestingly, the armchair CNNTs considered in our calculations displayed half metallic ground state. On the other hand, the zigzag tubes showed size dependency. In (5, 0) tube, the half metallic state was found, but the AFM state was stable in (4, 0) and (6, 0). Surprisingly, we found half metallic ground state in larger zigzag tubes of (7, 0), (8, 0), and (10, 0) indices. Due to lack of either theoretical or experimental evidences for chiral dependent magnetism of CNNTs, further investigation is necessary to confirm our results. Nonetheless, we have proposed a rule for magnetism of CNNTs. The armchair tube always prefers half metallic state. In contrast, the magnetic state of (n, 0) zigzag tube shows the diameter dependency in small tubes, but the zigzag tubes maintain half metallic state if the diameter is larger than that of (6, 0) tube. These results indicate that both armchair and zigzag tubes are likely to be half metallic, except for small tubes and this chirality independent half metallic feature will be greatly advantageous for spintronics applications. The *ab initio* molecular dynamics simulations reveal that the magnetic tube structure is stable at room temperature. Additionally, we have calculated the frequency dependent dielectric functions and absorption coefficients. In general, the absorption coefficient is larger in parallel polarization than in perpendicular polarization. More interestingly, we have obtained that the CNNTs are likely to be optically transparent in the range of visible light. This may imply that the CNNTs can be utilized in optical devices. Overall, the theoretical prediction for half metallicity without any external factor in one dimensional CNNTs may lead to new physics in spintronics and also other device applications because of potential multifunctional properties.

Methods

Vienna *ab initio* simulation package (VASP) was used[18–21]. Herein, the full potential projected plane wave framework[22,23] was used with an energy cutoff of 400 eV and the semi-local Perdew-Burke-Ernzerhof exchange-correlation functional[24] was employed. Structure optimization was performed using energy and force minimization procedures. Thus, all atoms have been fully relaxed until the force on each individual atom was smaller than 0.02 eV $Å^{-1}$. All calculations were performed based on using $1 \times 1 \times 9$ k-points. The CNNTs considered in our calculations are rolled up from two dimensional g-C_4N_3 layer in the perspective of the geometry. A building of CNNT has the same rule as applied for carbon nanotube. According to the labeling rule of tubular structures of carbon nanotube[25], the tube is defined by the chiral index (n, m) based on lattice vectors. The tubes with index (n, 0) is termed zigzag tube, while the tube labeled (n, n) is called armchair structure. To explore the effect of chirality on

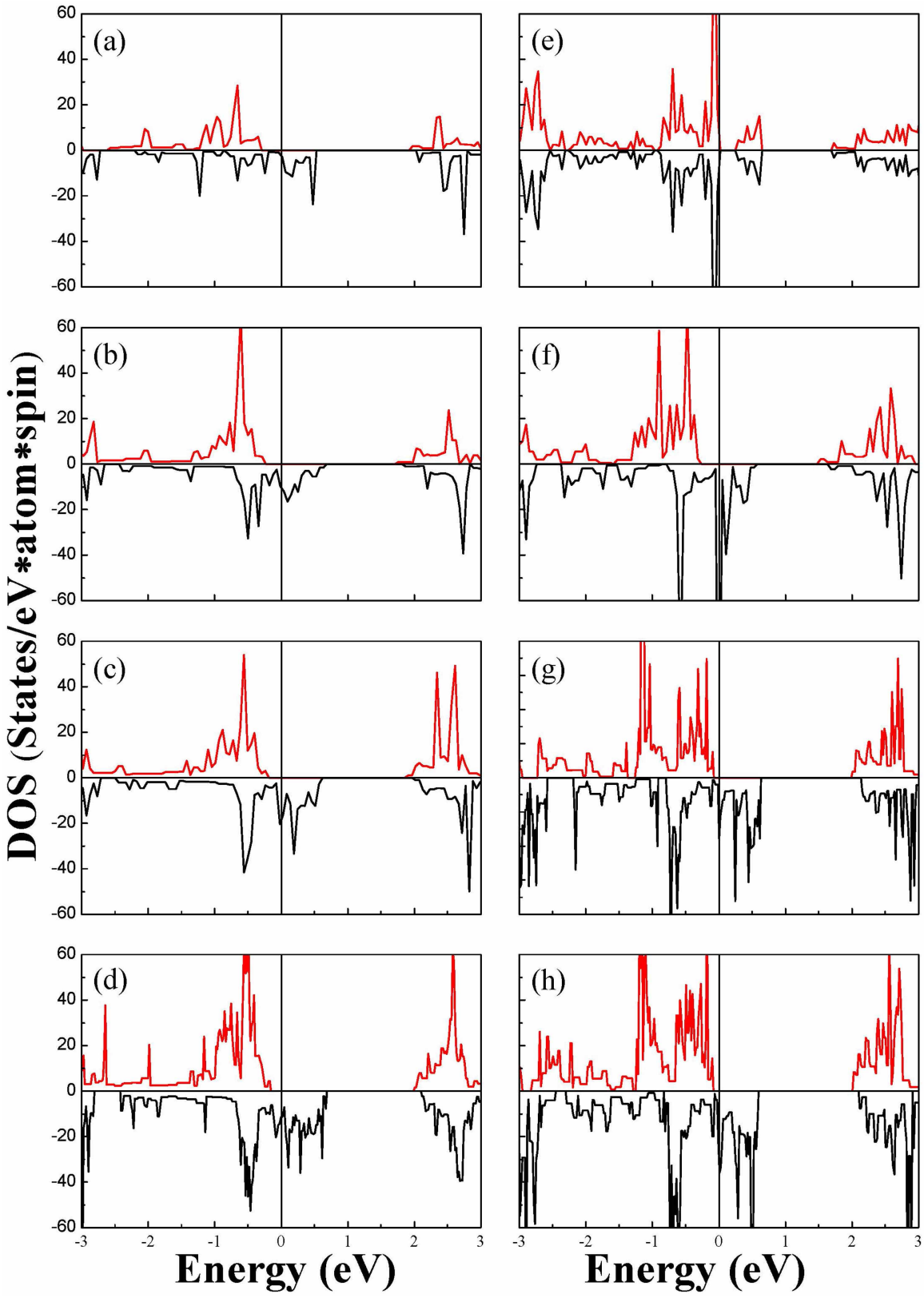

Figure 4 | Calculated total DOS: (a)–(d) are for (2, 2), (3, 3), (4, 4) and (6, 6) armchair tubes, respectively and (e)–(h) are for (4, 0), (5, 0), (7, 0) and (8, 0) zigzag tubes, respectively.

the magnetic property, we considered two types of CNNT such as armchair and zigzag structures. For zigzag CNNTs, six different structures with (4, 0), (5, 0), (6, 0), (7, 0), (8, 0), and (10, 0) are calculated and five armchair CNNTs of (2, 2), (3, 3), (4, 4), (5, 5), and (6, 6) structures are considered. The thermal stability was studied by using *ab initio* molecular dynamics. Here, we considered (4, 4) tube that contains 56 atoms and the molecular dynamics simulations were carried out at 300 and 500 K. Nosé–Hoover thermostat[26,27] was used to control the ionic temperature. The time-step is set as 1 fs.

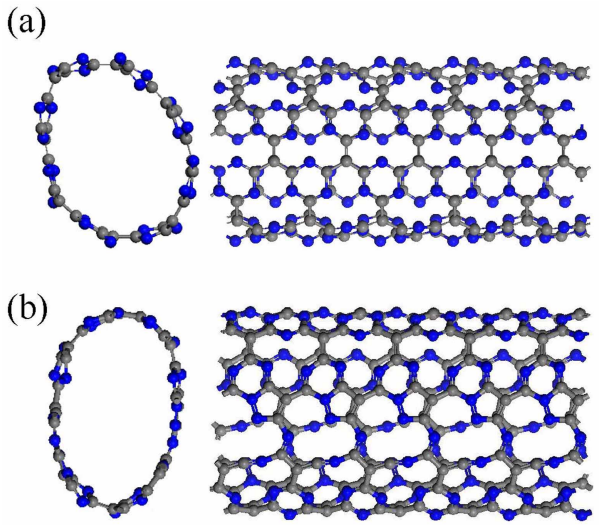

Figure 5 | Snapshots (Top and side view) at the end of 10 ps *ab initio* molecular dynamics simulation for tube (4, 4) at 300 K (a) and 500 K (b).

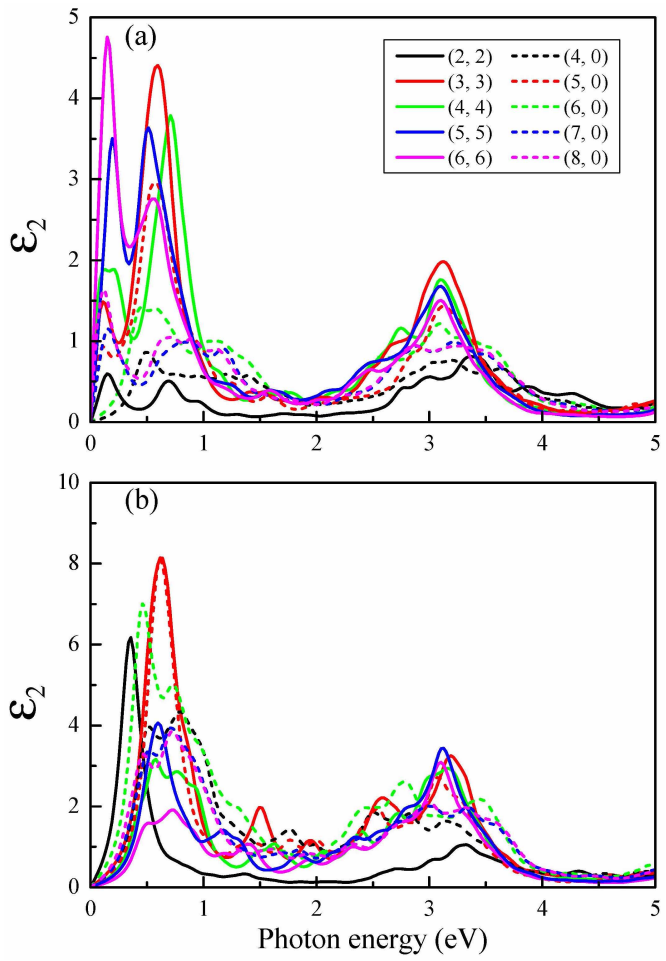

Figure 6 | Frequency dependent imaginary part of dielectric functions: (a) Perpendicular polarization to tube axis (b) Parallel polarization to tube axis.

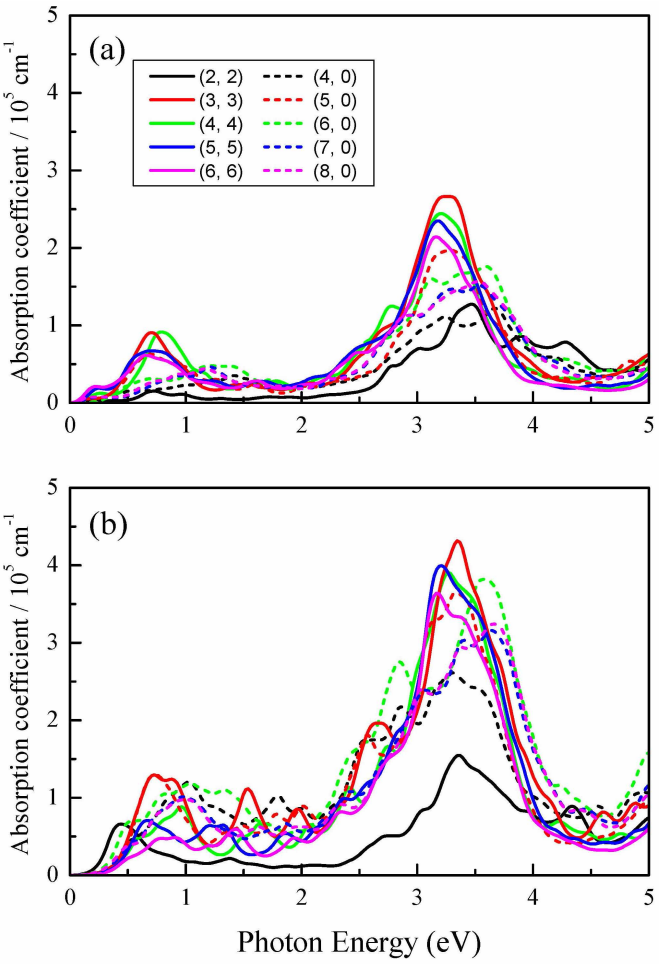

Figure 7 | Calculated absorption coefficients: (a) Perpendicular polarization to tube axis (b) Parallel polarization to tube axis.

1. Su, F., Antonietti, M. & Wang, X. mpg-C3N4 as a solid base catalyst for Knoevenagel condensations and transesterification reactions. *Catal. Sci. Technol.* **2**, 1005–1009 (2012).
2. Wang, X. *et al.* A metal-free polymeric photocatalyst for hydrogen production from water under visible light. *Nat. Mater.* **8**, 76–80 (2009).
3. Thomas, A. *et al.* Graphitic carbon nitride materials: variation of structure and morphology and their use as metal-free catalysts. *J. Mater. Chem.* **18**, 4893–4908 (2008).
4. Zheng, Y., Liu, J., Liang, J., Jaroniec, M. & Qiao, S. Z. Graphitic carbon nitride materials: controllable synthesis and applications in fuel cells and photocatalysis. *Energy Environ. Sci.* **5**, 6717–6731 (2012).
5. Xu, Y. & Gao, S.-P. Band gap of C3N4 in the GW approximation. *Int. J. Hydrog. Energy* **37**, 11072–11080 (2012).
6. Wang, X., Blechert, S. & Antonietti, M. Polymeric Graphitic Carbon Nitride for Heterogeneous Photocatalysis. *ACS Catal.* **2**, 1596–1606 (2012).
7. Lee, J. S., Wang, X., Luo, H. & Dai, S. Fluidic Carbon Precursors for Formation of Functional Carbon under Ambient Pressure Based on Ionic Liquids. *Adv. Mater.* **22**, 1004–1007 (2010).
8. Du, A., Sanvito, S. & Smith, S. C. First-Principles Prediction of Metal-Free Magnetism and Intrinsic Half-Metallicity in Graphitic Carbon Nitride. *Phys. Rev. Lett.* **108**, 197207 (2012).
9. Li, X., Zhang, S. & Wang, Q. Stability and physical properties of a tri-ring based porous g-C4N3 sheet. *Phys. Chem. Chem. Phys. PCCP* **15**, 7142–7146 (2013).
10. Li, Y., Sanvito, S. & Hou, S. Origin of the half-metallic properties of graphitic carbon nitride in bulk and confined forms. *J. Mater. Chem. C* **1**, 3655–3660 (2013).
11. Sun, S.-J. Interior edges induced half-metallic ferromagnetism in graphitic carbon nitride structures. *J. Magn. Magn. Mater.* **344**, 39–43 (2013).
12. Li, X., Zhou, J., Wang, Q., Kawazoe, Y. & Jena, P. Patterning Graphitic C–N Sheets into a Kagome Lattice for Magnetic Materials. *J. Phys. Chem. Lett.* **4**, 259–263 (2013).
13. Hashmi, A. & Hong, J. Metal free half metallicity in 2D system: structural and magnetic properties of g-C4N3 on BN. *Sci. Rep.* **4**, 4374 (2014).
14. Hashmi, A., Hu, T. & Hong, J. Transition from half metal to semiconductor in Li doped g-C4N3. *J. Appl. Phys.* **115**, 124312 (2014).

15. Gracia, J. & Kroll, P. First principles study of C3N4 carbon nitride nanotubes. *J. Mater. Chem.* **19**, 3020–3026 (2009).
16. Chai, G., Lin, C., Zhang, M., Wang, J. & Cheng, W. First-principles study of CN carbon nitride nanotubes. *Nanotechnology* **21**, 195702 (2010).
17. Pan, H., Zhang, Y.-W., Shenoy, V. B. & Gao, H. Metal-functionalized single-walled graphitic carbon nitride nanotubes: a first-principles study on magnetic property. *Nanoscale Res. Lett.* **6**, 97 (2011).
18. Kresse, G. & Hafner, J. Ab initio molecular dynamics for liquid metals. *Phys. Rev. B* **47**, 558–561 (1993).
19. Kresse, G. & Hafner, J. Ab initio molecular-dynamics simulation of the liquid-metal–amorphous-semiconductor transition in germanium. *Phys. Rev. B* **49**, 14251–14269 (1994).
20. Kresse, G. & Furthmüller, J. Efficiency of ab-initio total energy calculations for metals and semiconductors using a plane-wave basis set. *Comput. Mater. Sci.* **6**, 15–50 (1996).
21. Kresse, G. & Furthmüller, J. Efficient iterative schemes for ab initio total-energy calculations using a plane-wave basis set. *Phys. Rev. B* **54**, 11169–11186 (1996).
22. Blöchl, P. E. Projector augmented-wave method. *Phys. Rev. B* **50**, 17953–17979 (1994).
23. Kresse, G. & Joubert, D. From ultrasoft pseudopotentials to the projector augmented-wave method. *Phys. Rev. B* **59**, 1758–1775 (1999).
24. Perdew, J. P., Burke, K. & Ernzerhof, M. Generalized Gradient Approximation Made Simple. *Phys. Rev. Lett.* **77**, 3865–3868 (1996).
25. White, C. T., Robertson, D. H. & Mintmire, J. W. Helical and rotational symmetries of nanoscale graphitic tubules. *Phys. Rev. B* **47**, 5485–5488 (1993).
26. Nosé, S. A unified formulation of the constant temperature molecular dynamics methods. *J. Chem. Phys.* **81**, 511–519 (1984).
27. Hoover, W. G. Canonical dynamics: Equilibrium phase-space distributions. *Phys. Rev. A* **31**, 1695–1697 (1985).

Acknowledgments

This research was supported by Basic Science Research Program through the National Research Foundation of Korea (NRF) funded by the Ministry of Education, Science and Technology (No. 2013R1A1A2006071) and by the Supercomputing Center/Korea Institute of Science and Technology Information with supercomputing resources including technical support (KSC-2014-C3-015).

Author contributions

T.Hu and A.Hashmi are co-first authors and equally contributed to this work. J.H. reviewed and wrote the manuscript. T.H. prepared figure 1–4 and figure 7. A.H. prepared figure 5–6.

Additional information

Competing financial interests: The authors declare no competing financial interests.

How to cite this article: Hu, T., Hashmi, A. & Hong, J.S. Transparent half metallic g-C_4N_3 nanotubes: potential multifunctional applications for spintronics and optical devices. *Sci. Rep.* **4**, 6059; DOI:10.1038/srep06059 (2014).